

Photodissociation of nitric acid in a cold molecular beam at 193 nm

Peter Felder, Xuefeng Yang and J. Robert Huber

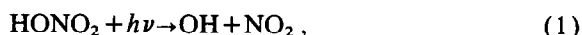
Physikalisch-Chemisches Institut der Universität Zürich, Winterthurerstrasse 190, CH-8057 Zurich, Switzerland

Received 16 August 1993; in final form 29 September 1993

The photodissociation of HONO₂ at 193 nm has been investigated by photofragment translational spectroscopy. Two competing primary dissociation processes were found: (1) HONO₂→OH+NO₂ (60%) and (2) HONO₂→HONO+O(¹D) (40%). The translational energy distribution of reaction (1) shows two components which correspond to the formation of stable and unstable (hot) NO₂ photofragments with a ratio of 1:2. The decay of hot NO₂ produces the secondary fragments NO+O(³P). The recoil anisotropy parameters associated with the respective dissociation processes $\beta(1) = -0.6 \pm 0.1$ and $\beta(2) = +0.6 \pm 0.2$ are consistent with an electronic transition dipole moment μ of the excitation which is oriented parallel to the line connecting the two terminal O atoms in the parent molecule.

1. Introduction

The photodissociation of nitric acid HONO₂ has received considerable attention mainly because of its atmospheric relevance [1,2], but also due to fundamental interest in the reaction dynamics of small molecules. For short reviews the reader is referred to the introductory sections of recent articles by Turnipseed et al. [3] and by Schiffmann et al. [4]. It is now well established [3,4] that photolysis of HONO₂ in the first absorption band centered near 260 nm proceeds according to the reaction



which has a dissociation energy $D_0^{(1)} = 47.6$ kcal/mol [5]. Characterization of this process was achieved by probing the nascent OH fragments with state-of-the-art laser spectroscopic techniques [6,7].

At shorter wavelength the absorption spectrum of HONO₂ shows a very strong band with a maximum at $\lambda \approx 185$ nm and an absorption cross section $\sigma_{185} \approx 2 \times 10^{-17}$ cm² [8]. Using the laser-induced fluorescence technique Wolfrum and co-workers [9] have probed the energy distribution of the OH fragments formed upon photolysis at 193 nm and found no detectable vibrational and only little rotational excitation. In addition to reaction (1), photolysis in

this strong absorption band involves a further dissociation channel, the identity and relative importance of which has still to be investigated. Turnipseed et al. [3] have measured the quantum yields for the formation of OH(X), O(³P), O(¹D) and H(²S) following irradiation at 248, 222 and 193 nm. For the latter wavelength they reported an OH production with a quantum yield $\phi(\text{OH}) = 0.33 \pm 0.06$. On the other hand, the quantum yield of O atom formation was found to be as high as 0.81 ± 0.13 , a result which was rationalized by the occurrence of two processes, namely



with $D_0^{(2)} = 117$ kcal/mol [5] and, to a lesser extent, the secondary dissociation of hot NO₂ formed in reaction (1):



Another primary dissociation channel which leads to H+NO₃ was found to be of marginal importance at 193 nm. Further support for reaction (2) was provided by Stuhl and co-workers [10], who observed in a pump-probe experiment a transient species which they attributed to HONO after careful consideration of all reasonable candidates. More recently, Nesbitt and co-workers have determined

$\phi(\text{OH})$ using flash kinetic spectroscopy with a tunable infrared laser [4]. Upon photolysis at 193 nm they found $\phi(\text{OH}) = 0.47 \pm 0.06$, which again directs attention to the presence of a decay channel other than reaction (1). However, a direct identification of this dissociation pathway is still lacking and, furthermore, very little is known about the partitioning of the excess energy among the degrees of freedom of the photofragments.

We have recently completed a detailed investigation on the photodissociation of methyl nitrate (CH_3ONO_2), the methyl ester of nitric acid [11]. Using photofragment translational spectroscopy (PTS) [12,13] we have established the presence of the reactions analogous to (1) and (2). In addition, we have characterized the energy disposal and the branching ratio of these reactions and observed the occurrence of secondary dissociation processes. The findings on methyl nitrate [11] motivated and supported our investigation of HONO_2 , the results of which are reported in this Letter.

2. Experiment

A description of our high-resolution photofragment translational spectrometer has been given elsewhere [14]. A pulsed molecular beam of HONO_2 seeded in helium was generated with a specially designed corrosion resistant valve driven by a piezoelectric translator [15]. Fuming nitric acid with a purity > 99.5% (Merck) was degassed to remove air and traces of NO_2 . A gas mixture of 8% was then formed by flowing He carrier gas with a stagnation pressure of 225 mbar through a liquid sample of HONO_2 cooled in an ice bath. The molecular beam velocity distribution $f(v) = C \exp[-(v-v_0)^2/\alpha^2]$ was determined by the laser-induced hole burning method [16] which yielded a most probable velocity $v_0 = 1200$ m/s and a width parameter $\alpha = 90$ m/s.

The photolysis at 193.3 nm was performed with an ArF excimer laser (lambda Physik EMG101 MSC) which was mildly focused at the intersection with the molecular beam. Measurements with the unpolarized laser were carried out with a fluence of 500 mJ/cm² or 50 mJ/cm², henceforth denoted as "high" and "low" power conditions, respectively. The photofragment recoil anisotropy [12,17] was obtained with

a linearly polarized photolysis laser (polarization degree 92%). All the time-of-flight (TOF) distributions have been corrected for the transit time of the ions through the mass filter.

3. Results and analysis

Photofragment TOF signals were detected with the mass filter settings $m/e = 16, 17, 30$ and 46. The interpretation was complicated by the highly efficient fragmentation of HONO and NO_2 in the electron bombardment ionizer and by the presence of products from secondary dissociation processes. To overcome these difficulties we proceeded as follows. Reaction (1) is known to occur and thus will certainly contribute to the signals at $m/e = 17$ (OH^+) and $m/e = 46$ (NO_2^+), but also at $m/e = 30$ (NO^+ from fragmentation of NO_2). Reaction (2) is expected to occur and should be manifested by a signal at $m/e = 16$ (O^+) and, although not very likely, at $m/e = 47$ (HONO^+), since HONO is known [18] to break down to form the daughter ions NO^+ and OH^+ , as well as some NO_2^+ . However, since the recoil velocities for the members of each photofragment pair are strictly correlated through the conservation of linear momentum, the OH^+ signals stemming from OH and HONO can be distinguished by taking into account the "momentum-matched" signals of their partner fragments NO_2 and O, respectively. The total translational energy distributions $P(E_T)$ in the center-of-mass (c.m.) frame of the fragment pairs were then obtained iteratively with a forward convolution method [19].

Neglecting the small residual internal energy of the parent molecules in the supersonic beam, the energy balance of the primary photodissociation process ($i = 1, 2$) is given by

$$E_{\text{avl}} = h\nu - D_0^{(i)} = E_T + E_A + E_B, \quad (4)$$

where $h\nu = 148$ kcal/mol is the photon energy at 193 nm, $D_0^{(i)}$ is the dissociation energy of reaction (i) and E_{avl} is the available energy which is partitioned between the translational energy E_T and the internal energies E_A and E_B of the two fragments A and B. The dissociation energies of reactions (1) and (2) are $D_0^{(1)} = 47.6$ kcal/mol [5] and $D_0^{(2)} = 117$ kcal/mol [5], respectively, assuming that reaction (2)

produces singlet oxygen atoms $O(^1D)$ (see section 4).

The TOF spectrum recorded at $m/e=17$ (OH^+) with the laboratory scattering angle $\theta=21^\circ$ and using the photolysis laser at low power is displayed in fig. 1a. It consists of two main signals with flight times of ≈ 100 and ≈ 240 μs , respectively. The earlier peak is split into two components labelled A and B; they are somewhat better resolved at $\theta=42^\circ$ shown in fig. 1b. As will be discussed below, the signals A and B can both be assigned to the OH fragments from re-

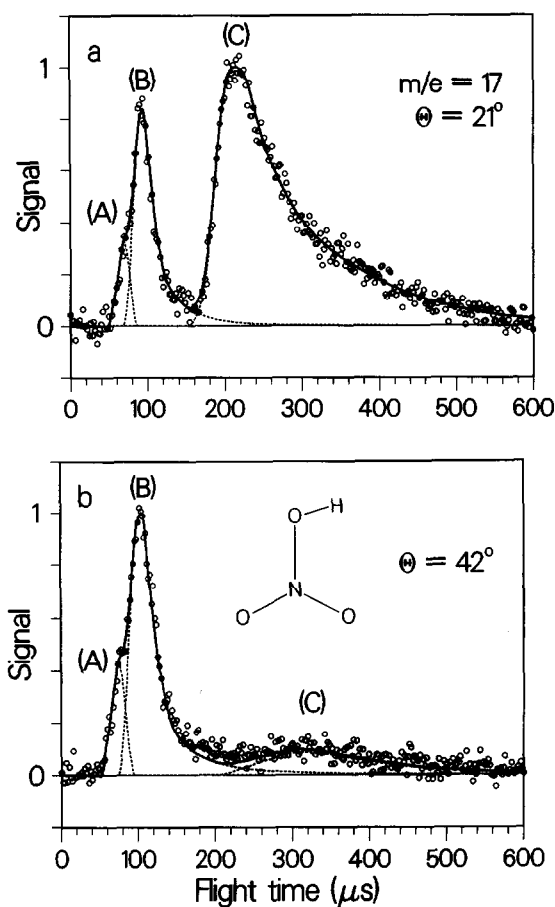


Fig. 1. TOF distributions measured at $m/e=17$ (OH^+) with $\theta=21^\circ$ (a) and 42° (b), following photodissociation of $HONO_2$ at 193 nm. Circles denote the experimental data and the solid line represents the best fit calculated with the $P(E_T)$ shown in fig. 2b (peaks A and B, $OH+NO_2$ channel) and fig. 2a (peak C, $HONO+O$ channel). The insert in the lower panel shows the planar equilibrium structure of the parent molecule in the electronic ground state.

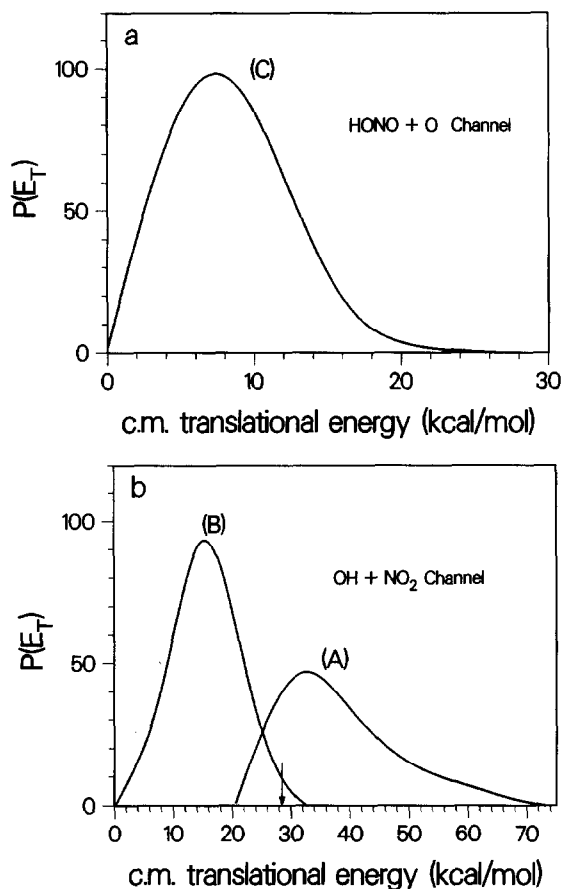


Fig. 2. Center-of-mass translational energy distribution $P(E_T)$ of the fragments from the photodissociation of $HONO_2$ at 193 nm, (a) $HONO+O(^1D)$ channel, corresponding to peak C of the TOF distributions in figs. 1 and 3. (b) $OH+NO_2$ channel, corresponding to peaks A and B of the TOF distributions in fig. 1. The arrow marks the threshold energy for secondary dissociation of NO_2 which is accessible if the translational energy of the $OH+NO_2$ fragment pair is smaller than $E_T^{thresh} = 28.5$ kcal/mol (see text).

action (1) while the broad peak labelled C is attributed to $HONO$ formed in (2). With this assignment we obtained the best-fitting $P(E_T)$ displayed in fig. 2; the corresponding fits of the TOF signals are shown as thick solid lines in figs. 1a and 1b. When the laser fluence was increased from 50 to 500 mJ/cm^2 , the shape of the TOF signal at $m/e=17$ remained essentially unchanged, but the intensity of peak C with respect to A and B decreased by about 10%. This ef-

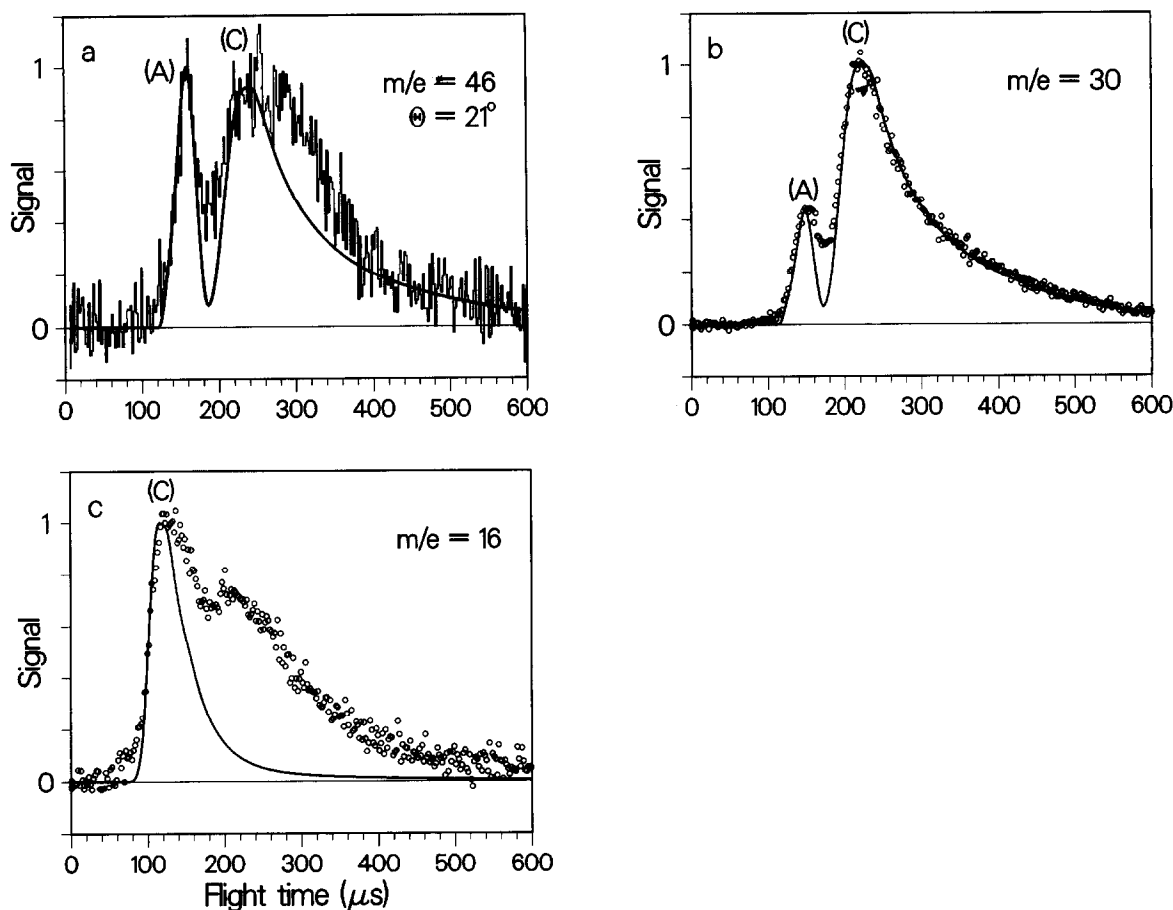


Fig. 3. TOF distributions measured at (a) $m/e=46$ (NO_2^+), (b) $m/e=30$ (NO^+), and (c) $m/e=16$ (O^+) with $\theta=21^\circ$. The solid lines in (a) and (b) were calculated with $P(E_T)$ of components A (stable NO_2 fragments) and C (HONO fragments) given in fig. 2, but without the component B (unstable NO_2 fragments). The solid line in (c) is the TOF spectrum of the O atoms from reaction (2) and was calculated with the $P(E_T)$ given in fig. 2a. Note that the TOF spectrum (a) was obtained with a reduced molecular beam velocity (1080 instead of 1200 m/s).

fect is consistent with the expectation that at higher laser power the secondary photodissociation of HONO becomes important.

Fig. 3a shows the TOF distribution at $m/e=46$ (NO_2^+) with $\theta=21^\circ$. The narrow peak at $\approx 160 \mu\text{s}$ is in good agreement with the signal calculated for component A of reaction (1) (see fig. 2b) and is therefore assigned to stable NO_2 product. However, no feature which would correspond to peak B in fig. 2b is observed at $m/e=46$. Considering the fact that any NO_2 produced with an internal energy exceeding $E_{\text{NO}_2}^{\text{thresh}} = D_0^{(3)} = 71.8 \text{ kcal/mol}$ [20] will rapidly de-

cay, and taking into account that the OH fragments from reaction (1) possess little internal energy [9], we find from the energy balance (4) that NO_2 with a translational energy of the fragment pair smaller than $\approx 28 \text{ kcal/mol}$ is unstable. ($E_{\text{T}}^{\text{thresh}} = h\nu - D_0^{(1)} - D_0^{(3)} = 148 - 47.6 - 71.8 = 28.6 \text{ kcal/mol}$). This threshold value in conjunction with the $P(E_T)$ of fig. 2b strongly indicates that peak B is due to the formation of OH fragments with an unstable NO_2 partner. Since the broad signal C at longer flight times in fig. 3a is also observed at $m/e=17$ and 30, and since a corresponding signal of the oxygen atom is

found at $m/e=16$ (see below), we assigned peak C to HONO formed in (2). Note however, that this signal also contains a small contribution from the products of the photodissociation of residual HONO₂ clusters which are inevitably present in the supersonic molecular beam.

The TOF spectrum at $m/e=30$ (NO⁺) with $\theta=21^\circ$ is exhibited in fig. 3b. The central portion of the peak at $\approx 140 \mu\text{s}$ stems from stable NO₂ fragments, as shown by the solid curve A which was calculated with the $P(E_T)$ pertaining to stable NO₂ (component A of fig. 2b). Secondary dissociation (3) of unstable NO₂ generates NO fragments which give rise to a broadening of the TOF peak. Because the slow and intense feature in fig. 3b is well reproduced by the signal calculated for reaction (2), it is identified as NO⁺ from HONO cracked in the detector. A further small signal at $\approx 100 \mu\text{s}$ was found to be strongly enhanced at higher excitation laser power and was therefore attributed to NO from the *photoinduced* secondary dissociation of NO₂ and HONO.

The reaction scheme including (1), (2) and (3) outlined so far is further supported by the TOF distribution measured at $m/e=16$ (O⁺) and shown in fig. 3c. The strong peak near $140 \mu\text{s}$ is due to oxygen atoms formed in reaction (2), whereas the broader signal with a maximum at $\approx 230 \mu\text{s}$ originates from the secondary O atoms produced in the decay of unstable NO₂. A part of this broad signal might also arise from O⁺ daughter ions of the HONO product. Finally, a power-dependent feature observed at early flight times in the TOF spectrum of fig. 3c is very probably the effect of O atoms formed via secondary photodissociation of NO₂.

The angular distribution of the photofragments in the c.m. frame is given by $w(\theta) \propto 1 + \beta P_2(\cos \theta)$, where P_2 is the second-order Legendre polynomial and θ is the angle between the electric vector of the laser light and the c.m. fragment recoil direction [17]. The anisotropy parameters β of the different dissociation processes and associated with the signals, A, B and C were derived from the relative intensities of the TOF signals measured at $m/e=17$ with $\theta=21^\circ$ and the laser polarization angles $\epsilon=-20^\circ, 25^\circ, 70^\circ$ and 115° . We obtained $\beta(A)=\beta(B)=-0.6 \pm 0.1$ and $\beta(C)=+0.6 \pm 0.2$.

Having established the $P(E_T)$ distributions and

the β parameters we are in the position to assess the relative importance of the primary dissociation channels. If the ionization cross sections and the mass spectra of HONO and OH are known, the integrated signal intensities of the three components in the TOF distribution measured at $m/e=17$ can be used to extract the branching ratio for the formation of these species according to the procedure described by Krajnovich et al. [21]. The ionization cross sections of HONO and OH were estimated from the relationship [22] $\sigma_{\text{ion}}=36 \times \alpha^{1/2}-18$, where σ_{ion} is the *maximum* ionization cross section (in units of \AA^2) which is expected to be approached with the electron energy of ≈ 100 eV used in our experiments. The molecular polarizability α [\AA^3] is approximated by the sum of the atomic polarizabilities found in the literature [23]. The ion cracking pattern of HONO was measured from the signal intensities of peak C at $m/e=17, 30$ and 46 , whereas for the OH fragment we expect no significant cracking. Based on these data we obtained the correction factors which, applied to the weighting factors derived from the TOF simulations, yielded the relative photodissociation yields for reactions (1) and (2) of 0.6 ± 0.1 and 0.4 ± 0.1 , respectively. Furthermore, in the case of reaction (1), the branching ratio between the two decay modes giving rise to peaks A and B is roughly 1:2 as estimated directly from the integrals of the corresponding $P(E_T)$ peaks shown in fig. 2b.

4. Discussion

Using the PTS method we have investigated the photodissociation of HONO₂ excited at 193 nm in a cold molecular beam. While the occurrence of reaction (2) as a process competing with reaction (1) has previously been proposed on the basis of indirect evidence [3,4,10], we have now been able to determine the recoil distributions of all the four primary product species formed in (1) and (2). From these data we have obtained an independent estimate of the branching ratio between reactions (1) and (2), have gained additional information on the dissociation dynamics of HONO₂ and, finally, have observed the existence of the secondary dissociation (3).

The relative yields of reactions (1) and (2) were

determined to be $\phi_1=0.6\pm 0.1$ and $\phi_2=0.4\pm 0.1$, respectively, with no evidence for other primary dissociation channels. Since fluorescence from the excited continuum of HONO₂ is negligible [24], our relative yields should be directly comparable with the results of the photochemical quantum yield measurements. The value $\phi_1=0.6$ is in reasonable agreement with the most recent one reported by Schiffmann et al. [4], who determined $\phi(\text{OH})=0.47\pm 0.06$. Furthermore, we found the relative yields of O(¹D) atom formation via reaction (2) and of O(³P) from the secondary dissociation of unstable NO₂ (component B of reaction 1) to be 0.4 each, which have to be compared with $\phi(\text{O}(\text{}^1\text{D}))=0.28\pm 0.13$ and $\phi(\text{O}(\text{}^3\text{P}))=0.53\pm 0.13$ determined by Turnipseed et al. [3].

In the case of reaction (1), an interesting new result emerges from our measurements of the translational energy release which reveals a bimodal $P(E_T)$ distribution (see fig. 2b) strongly indicating the existence of two distinct pathways A and B for reaction (1). Channel A produces OH+NO₂ pairs with an average kinetic energy of 38 kcal/mol which, according to the energy balance (4), corresponds to an average internal energy of 62 kcal/mol. The OH fragment is known to carry very little internal energy [9], but even if all the internal energy were channeled into the NO₂ product it would not be sufficient to overcome the barrier for unimolecular decay. Consequently, the NO₂ fragments formed in decay mode A should be *stable* and, indeed, we detected (undissociated) NO₂ at its parent ion mass $m/e=46$ (see fig. 3a). In contrast, channel B produces slower fragment pairs with an average internal energy of 84 kcal/mol so that the NO₂ fragments are expected to be *unstable*. This is confirmed by the fact that peak B, due to OH and NO₂ fragments, was observed at $m/e=17$ (OH fragment, fig. 1) but not at $m/e=46$ (NO₂ fragment, fig. 3a). Obviously, the secondary decay of NO₂ accounts for the relatively large yield of O(³P) atoms reported by Turnipseed et al. [3].

The nature of the two decay channels of (1) is not clear at present, but it is interesting to note that two distinct pathways for the formation of NO₂ have also been found in the case of the photodissociation of nitromethane (CH₃NO₂) [25] and methyl nitrate (CH₃ONO₂) [11]. Bai and Segal [26] have carried out calculations for the potential energy surfaces of

the four lowest singlet states of HONO₂. According to their results the photolysis at 193 nm accesses the third excited state S₃(2¹A') which is correlated with the fragment species OH(X)+NO₂($\tilde{\text{B}}^2\text{B}_1$) while the formation of ground state NO₂($\tilde{\text{X}}^2\text{A}_1$) requires internal conversion to one of the lower lying states S₁(1¹A'') or S₀(1¹A'). Since Suto and Lee [27] have determined the fluorescence quantum yield of electronically excited NO₂ photoproducts to be <0.5%, we have to conclude that the *stable* NO₂ product formed in pathway A is in the electronic ground state. For the competing and predominant pathway B, the formation of electronically excited NO₂($\tilde{\text{B}}^2\text{B}_1$) is conceivable (and consistent with the correlation [26]) but experimental evidence for such a species could not be provided because of the highly efficient unimolecular decay of NO₂. Therefore, we cannot rule out that *both* decay mechanisms A and B proceed indirectly via internal conversion to a lower electronic state. This possibility is consistent with the relatively low average kinetic energy release observed for both decay modes (38% and 16% of E_{avl} , respectively) and by our anisotropy measurements (see below).

The high efficiency of reaction (2) is remarkable in view of the large dissociation energy, $D_0^{(2)}=117$ kcal/mol as opposed to $D_0^{(1)}=47.6$ kcal/mol for reaction (1). The analogous behaviour was found in the case of the photodissociation of methyl nitrate [11], which appears to be a consequence of a localized photoexcitation of the nitro group in these two systems. While our detector does not allow us to distinguish between the ¹D and ³P states of the O atom, the following argument provides good evidence that reaction (2) forms the oxygen atoms predominantly in the singlet state. The translational energy distribution ranges from 0 to ≈ 20 kcal/mol with an average of 8 kcal/mol (see fig. 2a). For a given electronic state of the O atom, $P(E_T)$ directly reflects the internal energy distribution for the HONO fragments since, according to the energy balance (4), $E_{\text{HONO}}=E_{\text{avl}}-E_T$. If the oxygen atom were formed in the ground state O(³P), the available energy $E_{\text{avl}}=76$ kcal/mol would imply E_{HONO} to be between 56 and 76 kcal/mol, i.e. all the HONO fragments formed with partner O(³P) would have an internal energy well above the dissociation threshold $D_0(\text{HONO})=48$ kcal/mol [5]. However, since the $P(E_T)$

of reaction (2) was obtained from the TOF spectra of *undissociated* HONO fragments, we conclude that the oxygen atoms are created in a spin-allowed process yielding the excited electronic state 1D .

Finally, we address the anisotropy of reactions (1) and (2). The transition dipole moment μ of the $S_3(2^1A') \leftarrow S_0(1^1A')$ excitation lies in the molecular plane of HONO₂. Within C_{2v} symmetry obtained by treating the OH group as a pseudo-atom, the S_3 state has 1B_2 symmetry and μ is thus parallel to the line connecting the two terminal O atoms (see insert of fig. 1b). The measured β parameters are fully consistent with this orientation. For reaction (1) the recoil direction is approximately perpendicular to μ and, consequently, $\beta(A)$ and $\beta(B)$ should be close to -1 in the limit of prompt dissociation [28]. In reaction (2), on the other hand, the oxygen atom is expelled approximately along the direction of the breaking N–O bond which implies a positive β value, as is indeed observed. Furthermore, the calculated geometry of the S_3 state [26] predicts the angle between recoil direction and transition moment to be $\approx 34^\circ$, from which a limiting value [28] of $\beta(C) \approx 2 P_2(\cos 34^\circ) = 1.1$ is derived. The fact that the magnitudes of measured anisotropy parameters, $\beta(A) = \beta(B) = -0.6$ and $\beta(C) = +0.6$ are roughly half the respective limiting values is probably due to the lifetime of the excited state [28] and would, therefore, be consistent with an indirect (predissociation) mechanism.

Acknowledgement

Support by the Schweizerischer Nationalfonds zur Förderung der wissenschaftlichen Forschung and by the Alfred Werner Legat is gratefully acknowledged. We thank Dr. P. Willmott for critically reading the manuscript.

References

- [1] B.J. Finlayson-Pitts and J.N. Pitts, *Atmospheric chemistry* (Wiley, New York, 1973).
- [2] R.P. Wayne, *Chemistry of atmospheres* (Clarendon Press, Oxford, 1991).
- [3] A.A. Turnipseed, G.L. Vaghjiani, J.E. Thompson and A.R. Ravishankara, *J. Chem. Phys.* 96 (1992) 5887.
- [4] A. Schifmann Jr., D.D. Nelson and D.J. Nesbitt, *J. Chem. Phys.* 98 (1993) 6935.
- [5] JANAF, *Thermochemical Tables*, *J. Phys. Chem. Ref. Data* 14 (1985) Suppl. 1.
- [6] M. Brouard, S. Duxon, P.A. Enriquez and J.P. Simons, *J. Chem. Soc. Faraday Trans.* 89 (1993) 1435.
- [7] A. Sinha, R.L. Vander Wal and F.F. Crim, *J. Chem. Phys.* 91 (1989) 2929.
- [8] H.S. Johnston and R. Graham, *J. Phys. Chem.* 77 (1973) 62.
- [9] A. Jacobs, K. Kleinermanns, H. Kuge and J. Wolfrum, *J. Chem. Phys.* 79 (1983) 3162.
- [10] R.D. Kenner, F. Rohrer, T. Papenbrock and F. Stuhl, *J. Phys. Chem.* 90 (1986) 1294.
- [11] X. Yang, P. Felder and J.R. Huber, *J. Phys. Chem.*, in press.
- [12] G.E. Busch, R.T. Mahony, R.I. Morse and K.R. Wilson, *J. Chem. Phys.* 51 (1969) 449.
- [13] A.M. Wodtke and Y.T. Lee, in: *Molecular photodissociation dynamics*, eds. M.N.R. Ashfold and J.E. Baggott, (Royal Society of Chemistry, London, 1987) p. 31.
- [14] P. Felder, *Chem. Phys.* 143 (1990) 141.
- [15] M.-A. Thelen, P. Felder and J.R. Huber, *Chem. Phys. Letters* 213 (1993) 275.
- [16] T.K. Minton, P. Felder, R.J. Brudzynski and Y.T. Lee, *J. Chem. Phys.* 81 (1984) 1759.
- [17] R.N. Zare, *Mol. Photochem.* 4 (1972) 1.
- [18] X. Zhao, E.J. Hints and Y.T. Lee, *J. Chem. Phys.* 88 (1988) 801.
- [19] R.K. Sparks, K. Shobatake, L.R. Carlson and Y.T. Lee, *J. Chem. Phys.* 75 (1981) 3838.
- [20] U. Robra, H. Zacharias and K.H. Welge, *Z. Physik D* 16 (1990) 175.
- [21] D. Krajnovich, F. Huisken, Z. Zhang, Y.R. Shen and Y.T. Lee, *J. Chem. Phys.* 77 (1982) 5977.
- [22] R.E. Center and A. Mandl, *J. Chem. Phys.* 57 (1972) 4104.
- [23] T.M. Miller and B. Bederson, *Advan. At. Mol. Phys.* 13 (1977) 1.
- [24] W.B. DeMore, M.J. Molina, S.P. Sander, D.M. Golden, R.F. Hampson, M.J. Kurylo, C.J. Howard and A.R. Ravishankara (JPL Publication 87-41, Jet propulsion Laboratory, Pasadena, CA (1987).
- [25] L.J. Butler, D. Krajnovich, Y.T. Lee, G. Ondrey and R. Bersohn, *J. Chem. Phys.* 79 (1983) 1708.
- [26] Y.Y. Bai and G.A. Segal, *J. Chem. Phys.* 92 (1990) 7479.
- [27] M. Suto and L.C. Lee, *J. Chem. Phys.* 81 (1984) 1294.
- [28] S. Yang and R. Bersohn, *J. Chem. Phys.* 61 (1974) 4400.